Type of file: PDF
Size of file: 0 KB
Title of file for HTML: Supplementary Information
Description: Supplementary Figures.

Type of file: MP4
Size of file: 0 KB
Title of file for HTML: Supplementary Movie 1
Description: Proplatelet formation of wt MKs.

Type of file: MP4
Size of file: 0 KB
Title of file for HTML: Supplementary Movie 2
Description: Transmigration of $RhoA^{-/-}$ MKs.

Type of file: AVI
Size of file: 0 KB
Title of file for HTML: Supplementary Movie 3
Description: Intrasinusoidal adhesion of $RhoA^{-/-}$ MKs (1).

Type of file: MP4
Size of file: 0 KB
Title of file for HTML: Supplementary Movie 4
Description: Intrasinusoidal adhesion of $RhoA^{-/-}$ MKs (2).

Type of file: AVI
Size of file: 0 KB
Title of file for HTML: Supplementary Movie 5
Description: Release of large proplatelet-like fragments of $RhoA^{-/-}$ MKs.

Type of file: AVI
Size of file: 0 KB
Title of file for HTML: Supplementary Movie 6
Description: MK accumulation and reduced proplatelet formation of $RhoA/Cdc42^{-/-}$ MKs.

Type of file: PDF
Size of file: 0 KB
Title of file for HTML: Peer Review File
Description:

SUPPLEMENTARY INFORMATION

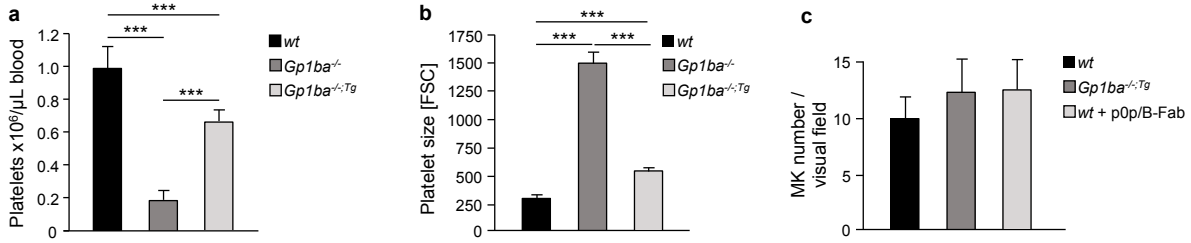

Supplementary Fig. 1. Macrothrombocytopenia in mice lacking functional GPIbα ectodomain. a, Reduced peripheral platelet count and **b,** increased platelet size in *Gp1ba*$^{-/-}$ (dark gray) and *Gp1ba*$^{-/-;Tg}$ (*Gp1ba-Tg,* light gray) mice compared to the *wt* (black) determined by flow cytometric analysis (n=4, 5, and 7). Results are representative of 3 independent experiments. **c,** Determination of MK numbers in immunolabeled BM sections from *wt* (black), *Gp1ba*$^{-/-;Tg}$ (dark gray) and *wt* mice after treatment with GPIbα-blocking monovalent Fab fragments, p0p/B-Fab (light gray) (n=4, 7, 5). Bar graphs represent mean ± SD. Two-way ANOVA with Bonferroni correction for multiple comparisons; ***P < 0.001.

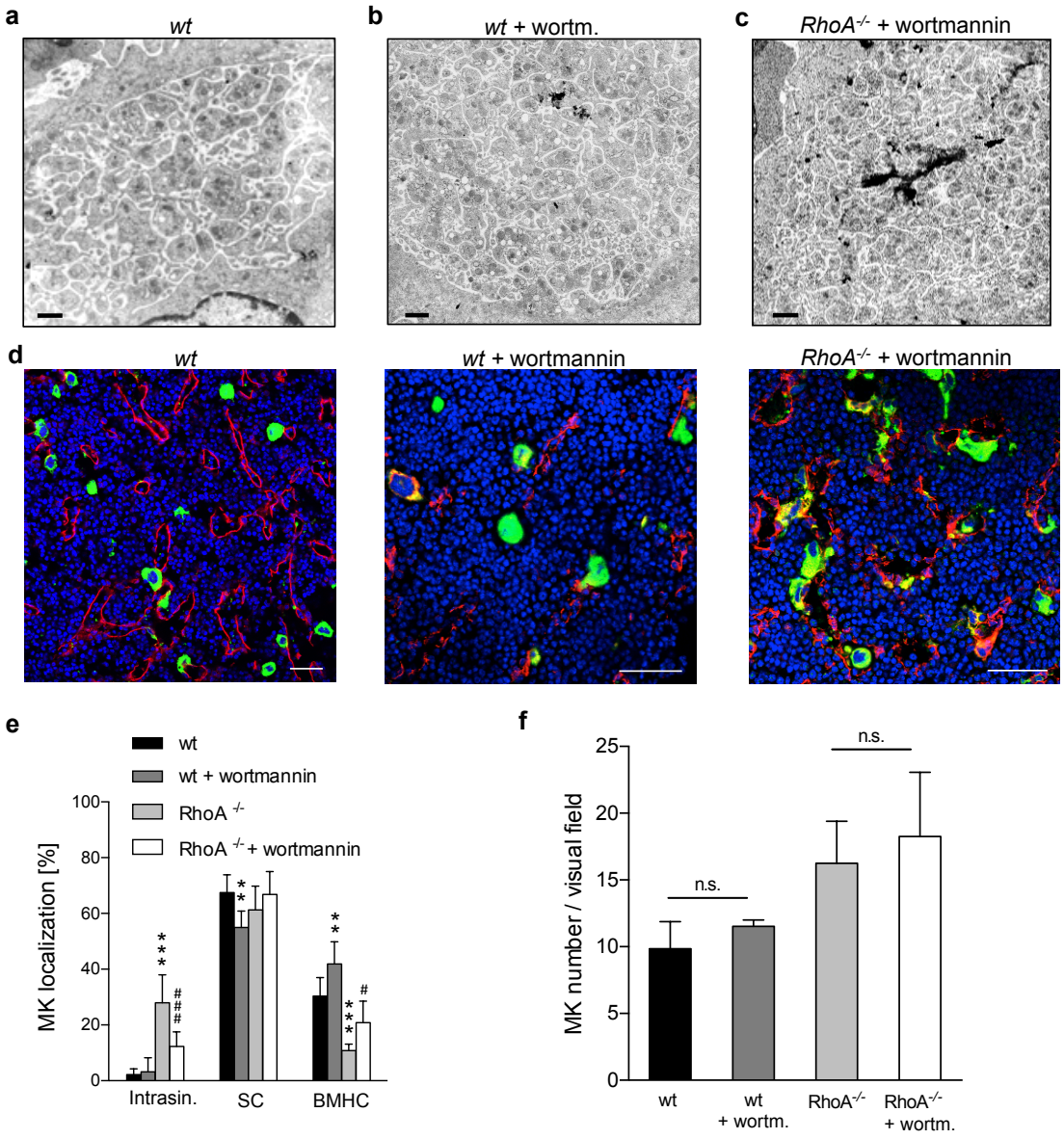

Supplementary Fig. 2. PI3K inhibition by wortmannin alters MK localization in the BM. **a-c,** TEM analysis of BM MKs of *wt* mice (**a**), and *wt* as well as *RhoA*$^{-/-}$ mice after treatment with the PI3K inhibitor wortmannin (**b,c**). Scale bars, 2 µm (**a-c**). **d,** Representative confocal images of immunostained BM MKs of *wt* mice and *wt* as well as *RhoA*$^{-/-}$ mice after treatment with wortmannin. Results are representative of 2 independent experiments. Scale bars, 50 µm. MKs, proplatelets and platelets are shown by GPIX staining in green. Endoglin staining (red) labels vessels. DAPI, blue. **e,** Quantification of MK localization in the BM reveals reduced sinusoidal contact (SC) in *wt* mice (dark gray) and reduced intrasinusoidal localization of *RhoA*$^{-/-}$ MKs (white) upon wortmannin treatment compared to the *wt* (black)

and untreated *RhoA*$^{-/-}$ mice (light gray), respectively (n=5, 6, 10, and 9). Results are pooled from 2 independent experiments. **f,** Determination of MK numbers in immunolabeled BM sections from wt and *RhoA*$^{-/-}$ mice, as well as *wt and RhoA*$^{-/-}$ mice after treatment with wortmannin (n=3, 5, 9, 6). Bar graphs represent mean ± SD. Two-way ANOVA with Bonferroni correction for multiple comparisons; $^{**}P < 0.01$; $^{***}P < 0.001$ compared to *wt*; $^{\#}P < 0.05$; $^{\#\#\#}P < 0.001$ compared to *RhoA*$^{-/-}$. n.s., not significant.

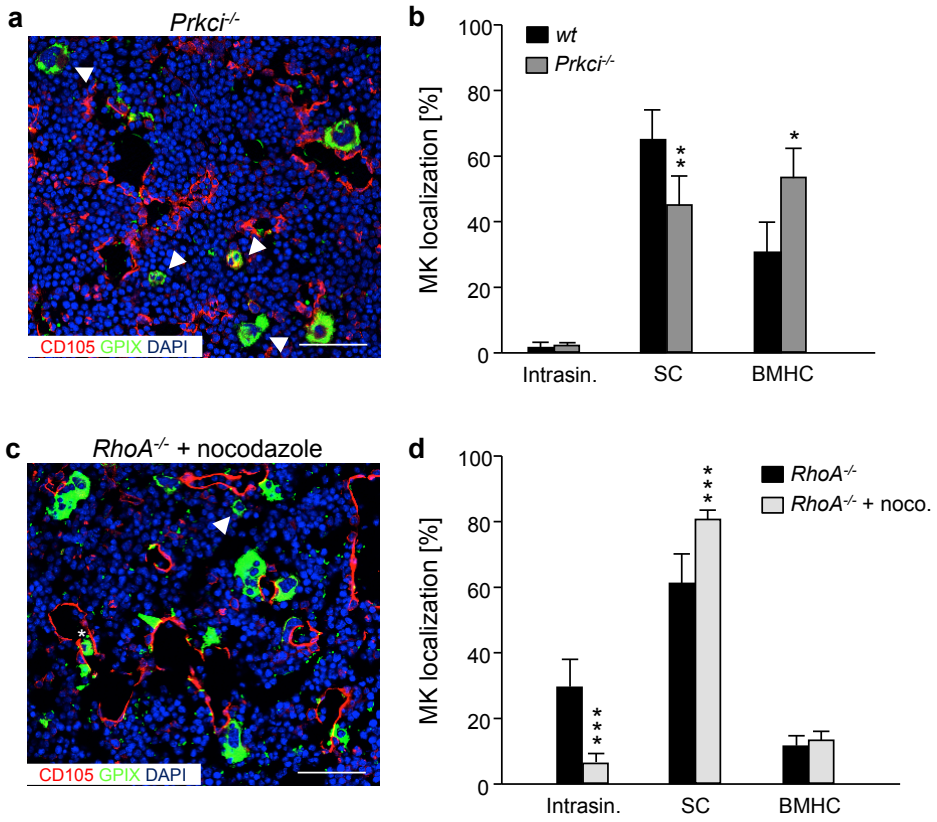

Supplementary Fig. 3. PKCι-deficiency reduces sinusoidal contact of BM MKs and microtubule disruption reverts intrasinusoidal localization of *RhoA*$^{-/-}$ MKs. a, Representative confocal images of immunostained BM of *Prcki*$^{-/-}$ mice. Scale bar, 50 µm. MKs, proplatelets and platelets are shown by GPIX staining in green color. Endoglin staining (red) labels vessels. DAPI, blue. Arrowhead indicates MKs in BMHC. **b,** Quantification of MK localization in the BM of wt (black) and *Prcki*$^{-/-}$ mice (dark gray) (n=4 and 7). **c,** Representative confocal image of immunostained BM of *RhoA*$^{-/-}$ mice after treatment with nocodazole. Scale bar, 50 µm. Arrowhead indicates MKs in BMHC, asterisk indicates intrasinusoidal (intrasin.) MKs. **d,** Quantification of MK localization in the BM of *RhoA*$^{-/-}$ mice (black) and nocodazole-treated *RhoA*$^{-/-}$ mice (light gray) (n=4). Bar graphs represent mean ± SD. Two-way ANOVA with Bonferroni correction for multiple comparisons; ***$P < 0.001$, **$P < 0.01$, *$P < 0.05$.

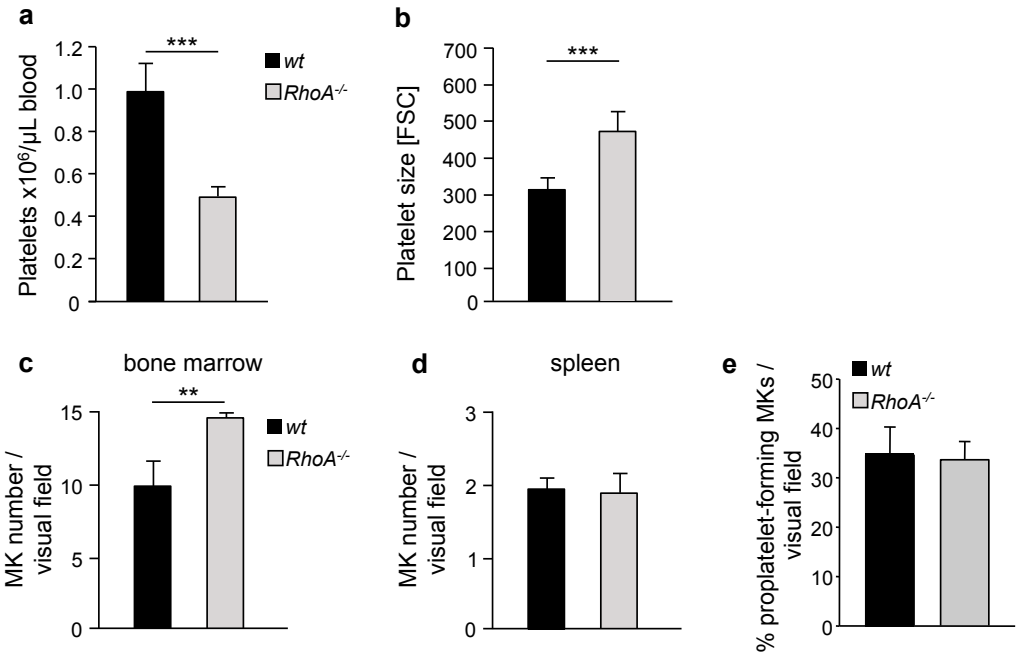

Supplementary Fig. 4. Macrothrombocytopenia and increased MK number in the BM of *RhoA*$^{-/-}$ mice. a, Reduced peripheral platelet count and **b,** increased platelet size in *RhoA*$^{-/-}$ mice (light gray) compared to the *wt* (black), as determined by flow cytometric analysis (n=7 and 5). Results are representative of 5 independent experiments. **c, d,** Determination of MK numbers in hematoxylin and eosin–stained BM (**c**) and spleen (**d**) sections from *wt (black)* and *RhoA*$^{-/-}$ mice (light gray) (n=4 and 7). Bar graphs represent mean ± SD. Unpaired two-tailed Student's *t*-test; $^{**}P < 0.01$; $^{***}P < 0.001$.

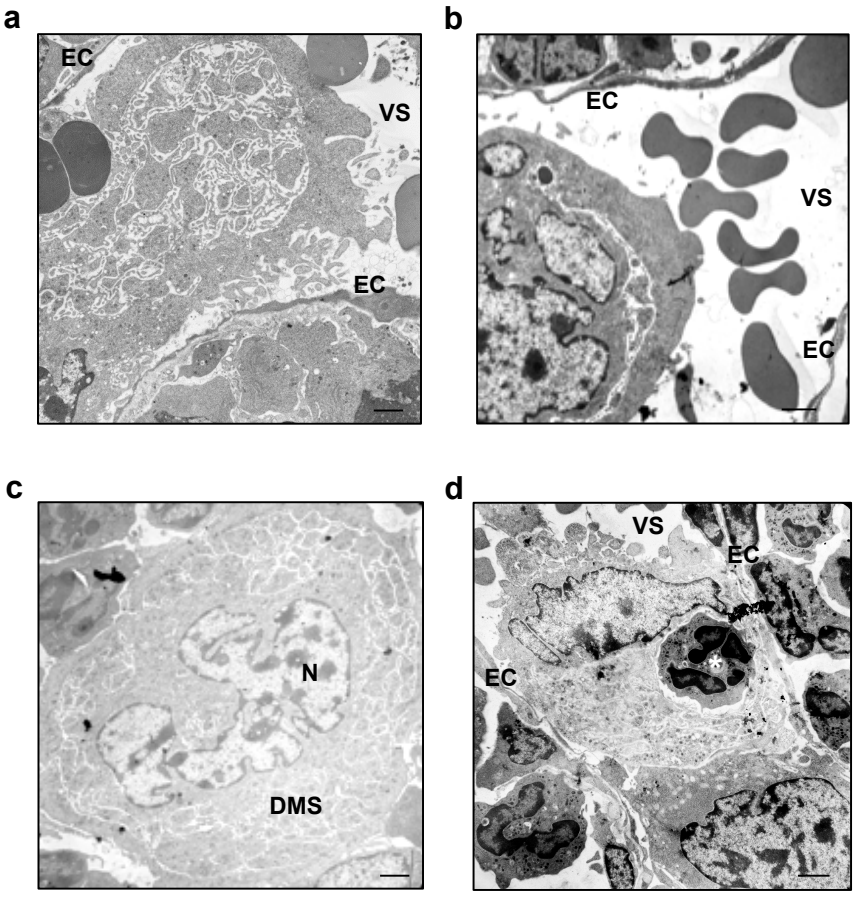

Supplementary Fig. 5. Normal DMS formation, but intrasinusoidal localization of *RhoA*$^{-/-}$ MKs in the BM. a, b, TEM analysis of *RhoA*$^{-/-}$ BM MKs reveals MKs adherent to endothelial cells (ECs) inside BM sinusoids (**a**) containing poly-lobulated nuclei (**b**). **c,** DMS formation was unaltered in *RhoA*$^{-/-}$ MKs. **d,** MK showing emperipolesis (indicated by asterisk; n=8). Scale bars, 2.5 µm. EC, endothelial cell; VS, vascular sinus; N, nucleus; DMS, demarcation membrane system.

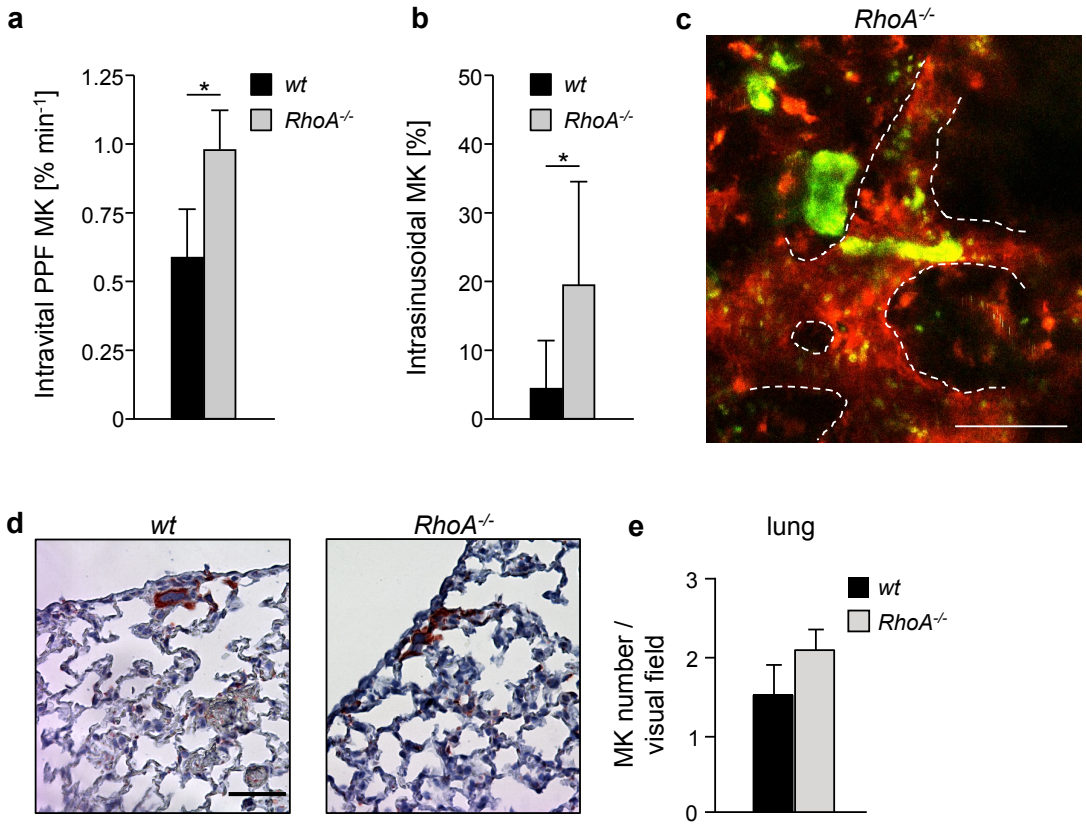

Supplementary Fig. 6. Increased proplatelet-formation and intrasinusoidal localization of *RhoA*$^{-/-}$ MKs. a, Quantification of proplatelet-forming (PPF) MKs per minute and **b,** Quantification of intrasinusoidal MKs in *wt* (black) and *RhoA*$^{-/-}$ (light gray) mice (n=7 and 4). **c,** Representative image showing intravital two-photon microscopy of BM *RhoA*$^{-/-}$ MKs in the skull. Scale bars, 50 µm. **d,** Histological analysis of lungs from *wt* (left) and *RhoA*$^{-/-}$ (right) mice. MKs are shown by GPIbα-HRP staining, sections were counterstained with hematoxylin. Scale bar, 50 µm. **e,** Quantification of MK number in *wt* (black) and *RhoA*$^{-/-}$ (light gray) mice in the lung (n=4 and 5). Bar graphs represent mean ± SD. Unpaired two-tailed Student's *t*-test; **P* < 0.05.

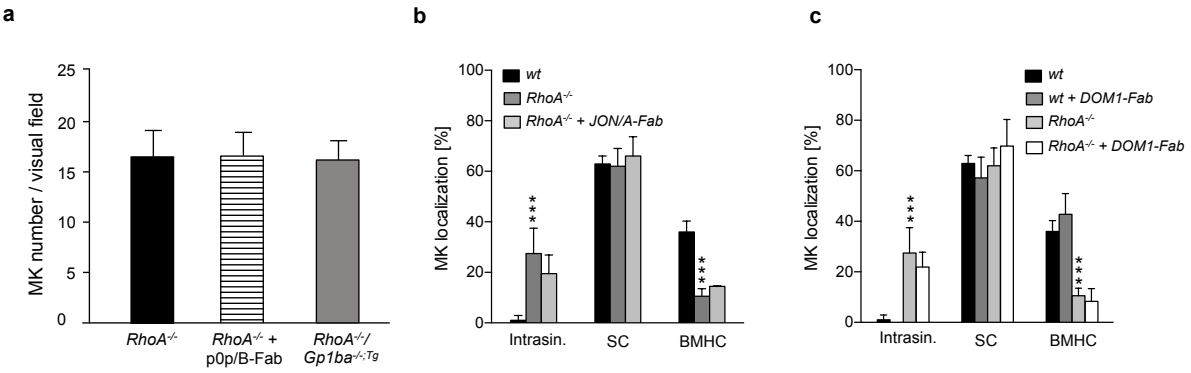

Supplementary Fig. 7. MK number in the BM of *RhoA*$^{-/-}$ mice after GPIbα blockade and MK localization in *wt* and *RhoA*$^{-/-}$ mice after treatment with Fab fragments directed against integrin αIIbβ3 and GPV. a, Unaltered MK number in the BM of *RhoA*$^{-/-}$ mice after treatment with GPIbα-blocking monovalent Fab fragments, p0p/B-Fab (light gray), or upon concomitant lack of the GPIbα ectodomain (*RhoA*$^{-/-}$*/Gp1ba*$^{-/-;Tg}$; dark gray) compared to the *wt* (black). n=8, 3, and 9). **b, c,** Quantification of MK localization in the BM of *wt* (black) and *RhoA*$^{-/-}$ mice (light gray) after treatment with monovalent Fab fragments directed against integrin αIIbβ3 (JON/A) **(b)** or GPV (DOM1) **(c)** (n=3, 1 experiment). The vehicle-treated *wt* is shown in black. Bar graphs represent mean ± SD. Two-way ANOVA with Bonferroni correction for multiple comparisons; ***$P < 0.001$.

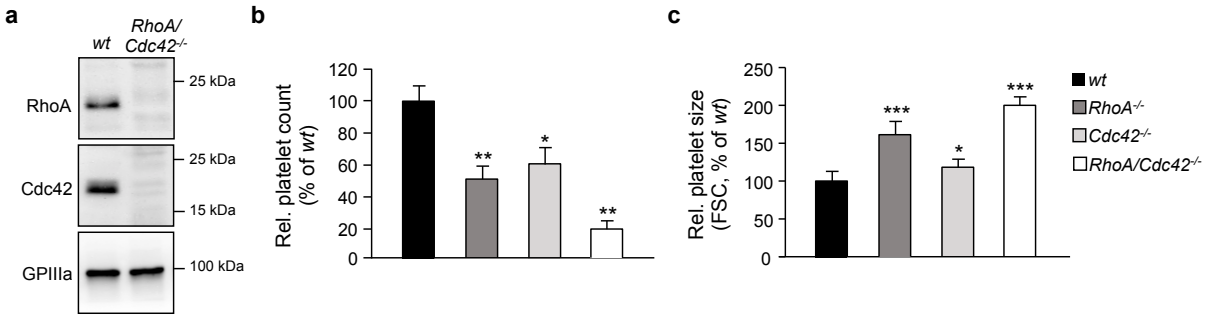

Supplementary Fig. 8. Severe macrothrombocytopenia in the absence of RhoA and Cdc42 in MKs. a, Western blot analysis of RhoA and Cdc42 expression in *wt* and *RhoA/Cdc42*$^{-/-}$ platelets. GPIIIa expression was used as loading control. Results shown are representative of 3 independent experiments. **b, c,** Analysis of peripheral platelet count (**b**) and size (**c**) in *wt* (black), *RhoA*$^{-/-}$ (dark gray), *Cdc42*$^{-/-}$ (light gray), and *RhoA/Cdc42*$^{-/-}$ (white) mice (n=4). Results shown are representative of 3 independent experiments. Bar graphs represent mean ± SD. Two-way ANOVA with Bonferroni correction for multiple comparisons; **P* < 0.05; ***P* < 0.01; ****P* < 0.001.

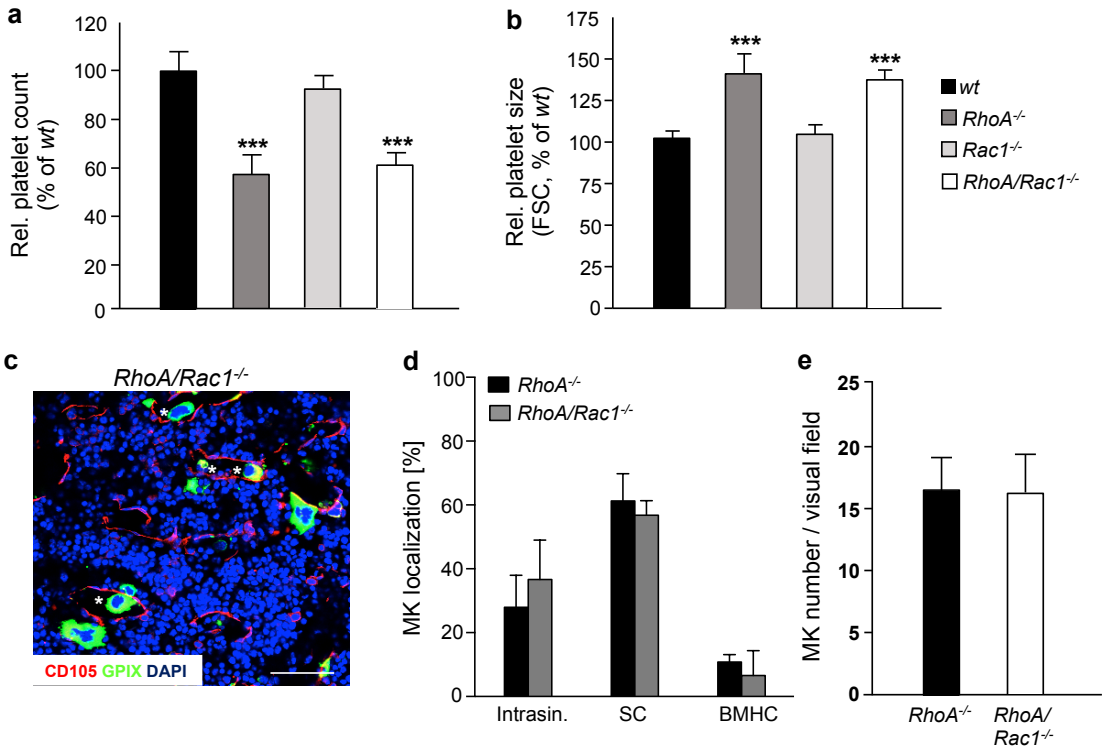

Supplementary Fig. 9. Concomitant loss of Rac1 does not influence megakaryopoiesis in *RhoA*$^{-/-}$ mice. a, b, Analysis of peripheral platelet count (**b**) and size (**c**) in *wt* (black), *RhoA*$^{-/-}$ (dark gray), *Rac1*$^{-/-}$ (light gray), and *RhoA/Rac1*$^{-/-}$ (white) mice (n=4). Results are representative of 3 independent experiments. **c,** Representative confocal images of immunostained BM of *RhoA/Rac1*$^{-/-}$ mice. MKs, proplatelets and platelets are shown by GPIX staining in green color. Endoglin staining (red) labels vessels. DAPI, blue. Asterisk indicates intrasinusoidal (intrasin.). Scale bar, 50 µm. **d,** Quantification of MK localization in the BM of *wt* (black) and *RhoA/Rac1*$^{-/-}$ (dark gray) mice (n=9 and 3). **e,** Determination of MK numbers in hematoxylin and eosin–stained BM of *RhoA*$^{-/-}$ (black) and *RhoA/Rac1*$^{-/-}$ (white) mice. Bar graphs represent mean ± SD. Two-way ANOVA with Bonferroni correction for multiple comparisons; ***$P < 0.001$.

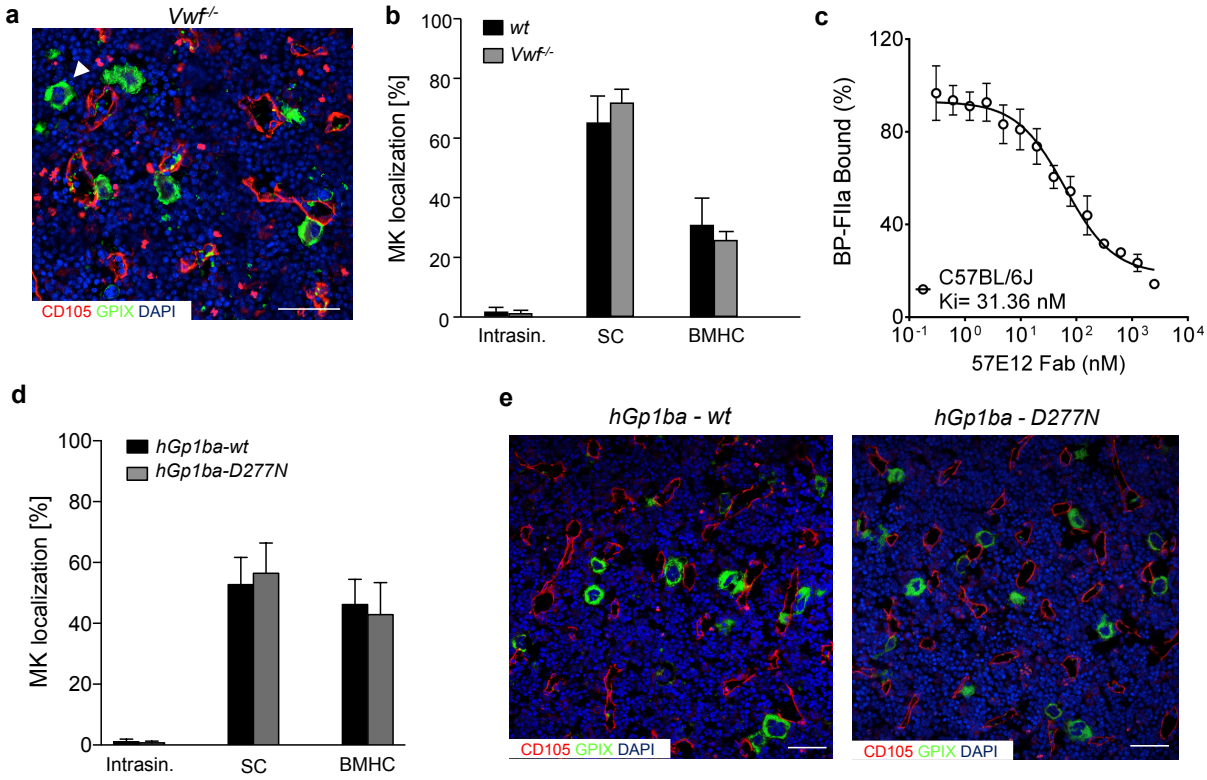

Supplementary Fig. 10. Deficiency of vWF or mutation of the thrombin binding site in mice expressing human GP1bα does not affect the localization of BM MKs. a, Representative confocal images of immunostained BM of *Vwf*$^{-/-}$ mice. Scale bar, 50 µm. MKs, proplatelets and platelets are shown by GPIX staining in green color. Endoglin staining (red) labels vessels. DAPI, blue. Arrowhead indicates MKs in BMHC. **b,** Quantification of MK localization in the BM of wt (black) and *Vwf*$^{-/-}$ (dark gray) mice (n=4 and 5). **c,** Monovalent p0p/B-Fab fragments inhibit binding of thrombin (FIIa) to GPIbα. **d,** MK localization in the BM is similar in mice expressing wt (*hGp1ba-wt*) or mutant (*hGp1ba-D277N*) GPIbα unable to bind thrombin (n=3). **e**, Representative confocal images of immunostained BM of transgenic mice harboring *hGp1b-wt* or *hGp1ba-D277N*. Scale bars, 50 µm. MKs, proplatelets and platelets are shown by GPIX staining in green color. Endoglin staining (red) labels vessels. DAPI, blue. Bar graphs represent mean ± SD.

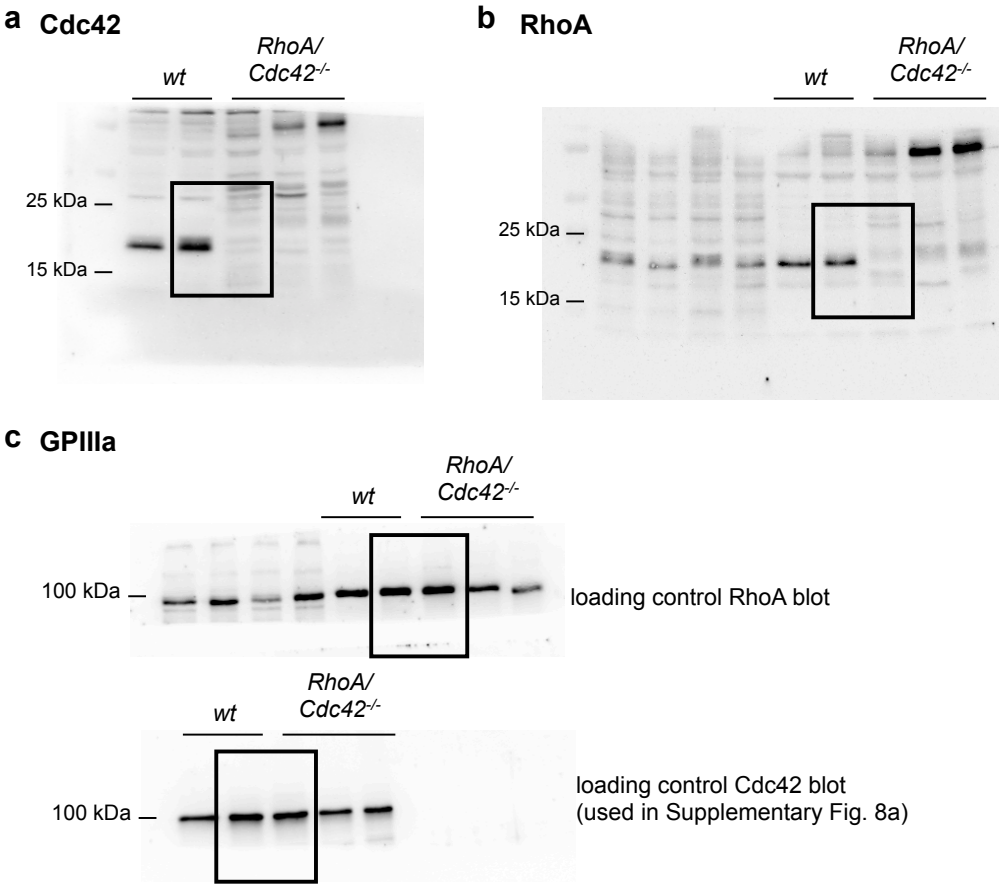

Supplementary Fig. 11. Uncropped Western blot images. Western blot analysis of Cdc42 (**a**), RhoA (**b**) and GPIIIa (loading control, **c**) expression in platelet lysates from *wt* and *RhoA/Cdc42*$^{-/-}$ mice. Cropped versions of these images are shown in Supplementary Fig. 8a. Genotypes, molecular weight markers, and selected lanes are depicted.